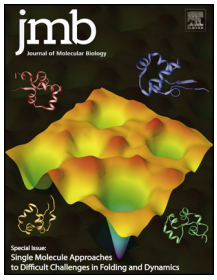

A Survey of DDX21 Activity During Rev/RRE Complex Formation

John A. Hammond [1,†], Li Zhou [1,†], Rajan Lamichhane [1], Hui-Yi Chu [2], David P. Millar [1], Larry Gerace [2] and James R. Williamson [1]

*1 - **Department of Integrative Structural and Computational Biology,** The Scripps Research Institute, La Jolla, CA 92037, USA*
*2 - **Department of Molecular Medicine,** The Scripps Research Institute, La Jolla, CA 92037, USA*

***Correspondence to James R. Williamson:** jrwill@scripps.edu*
http://dx.doi.org/10.1016/j.jmb.2017.06.023
Edited by M. F. Summers

Abstract

HIV-1 requires a specialized nuclear export pathway to transport unspliced and partially spliced viral transcripts to the cytoplasm. Central to this pathway is the viral protein Rev, which binds to the Rev response element in stem IIB located on unspliced viral transcripts and subsequently oligomerizes in a cooperative manner. Previous work identified a number of cellular DEAD-box helicases as *in vivo* binding partners of Rev, and siRNA experiments indicated a functional role for many in the HIV replication cycle. Two DEAD-box proteins, DDX1 and DDX3, had previously been shown to play a role in HIV pathogenesis. In this study, another protein identified in that screen, DDX21, is tested for protein and RNA binding and subsequent enzymatic activities in the context of the Rev/RRE pathway. We found that DDX21 can bind to the RRE with high affinity, and this binding stimulates ATPase activity with an enzymatic efficiency similar to DDX1. Furthermore, DDX21 is both an ATP-dependent and ATP-independent helicase, and both ATPase and ATP-dependent helicase activities are inhibited by Rev in a dose-dependent manner, although ATP-independent helicase activity is not. A conserved binding interaction between DDX protein's DEAD domain and Rev was identified, with Rev's nuclear diffusion inhibitory signal motif playing a significant role in binding. Finally, DDX21 was shown to enhance Rev binding to the RRE in a manner similar to that previously described for DDX1, although DDX3 does not. These data indicate that DDX1 and DDX21 have similar biochemical activities with regard to the Rev/RRE system, while DDX3 differs.

Background

During HIV replication, transcription of proviral DNA is functionally linked to the splicing, export, and translation of HIV RNA. The early protein regulator of expression of virion proteins, Rev, is transported into the nucleus and binds to the Rev-responsive element (RRE) RNA located in the *env* gene of unspliced or singly spliced viral RNA transcripts. This results in transport of those RNAs from the nucleus to the cytoplasm *via* the host cell CRM-1 export pathway [1].

Rev is a 116-amino acid (aa) protein, with a structured N-terminus responsible for RNA binding, Rev oligomerization, and nuclear import, and an unstructured C-terminus responsible for nuclear export (Fig. 1a). The shuttling of Rev between the cytoplasm and the nucleus occurs by temporally controlled engagement of either the nuclear localization signal or nuclear export signal. Rev monomers bind to the RRE RNA *via* a high-affinity binding site located within stem II (Fig. 1b) and subsequently oligomerize in a stepwise and cooperative manner [2–9]. This oligomerized RNP product is the substrate for binding to CRM-1, resulting in export of the viral transcript from the nucleus.

While many cellular components of the CRM-1 export machinery have been characterized, other factors that might be involved in Rev-related functions are still not well understood. Work to identify other Rev cofactors led to the identification of a number of DEAD-box helicases that are able to interact with Rev-containing complexes (RCCs) intracellularly [10]. Two of these DEAD-box helicases, DDX1 and DDX3,

had been previously implicated in the HIV-1 Rev regulatory pathway [10–22]. DDX1 directly interacts with Rev and RCCs, playing a role in the correct localization of Rev within the nucleus *in vivo*, as well as affecting Rev's association with and oligomerization on the RRE *in vitro* [10,12,14,15,23,24]. DDX3 affects HIV production at the mRNA export, protein translation, and budding steps of the viral life cycle, although what role, if any, Rev may play in these processes remains unclear [10,18,19,21]. The roles of the other helicases that were found to interact with Rev, including DDX21, have not been fully characterized, nor have their biophysical interactions with or biochemical implications to Rev and Rev-dependent processes.

DDX21, also known as nucleolar RNA helicase 2 and Gu, is highly expressed in various types of cancers [25,26] and is implicated in multiple steps of ribosome biogenesis, namely, rRNA processing [27], coordination between transcription and rRNA processing [28], and the recruitment of snoRNAs into pre-ribosome complexes [29]. DDX21 also inhibits influenza A viral replication by interacting with viral PB1 protein and inhibiting the viral RNA polymerase [30] and has been implicated in the dsRNA response in dendritic cells [31]. Previous immunoprecipitation (IP) experiments followed by phenotypic characterization of protein knockdown indicated that HIV requires DDX21 for efficient viral production [10]. Furthermore, this DDX21-dependent viral activity was shown to affect the distribution of unspliced RNA in the cell, similar to that seen with DDX1, and therefore may be a functional partner for Rev-related processes [10]. The DDX21 protein contains all the signature motifs (Q, I–VI) required for DEAD-helicase function (Fig. 1c) (for a review of DEAD-box helicases, see Ref. [32]). In addition to the conserved helicase core domains seen in DDX1 and DDX3, DDX21 contains several atypical FRGQR repeats located in its C-terminus that contribute to its RNA binding and RNA folding activities [33,34].

In this study, the RNA-dependent ATPase, RNA binding, and protein binding activities of DDX21 are compared to the previously published results for DDX1 and DDX3 [13,23,35]. Furthermore, these activities are discussed in the context of the Rev/RRE regulatory pathway, including the effect of each helicase on Rev oligomerization on the RRE.

Results

DDX21 is an RNA-stimulated ATPase

Previous work established both DDX1 and DDX3 as RNA-stimulated ATPases [13]. For DDX1, this activity was stimulated by various RNAs including tRNA, RRE RNA, and stem IIB RRE RNA (the high-affinity binding site of Rev). DDX21 ATP hydrolysis activity was measured using a steady-state assay where ATP hydrolysis is enzymatically coupled to the oxidation of NADH *via* pyruvate kinase and lactate dehydrogenase [36]. The consumption of NADH is optically monitored at 340 nm as a read-out of ATPase activity. Steady-state kinetic assays were carried out while titrating the ATP concentration in the presence of saturating amounts of stem IIB RNA (Fig. 2a). The k_{cat} for ATP hydrolysis was 0.67 min^{-1} with a K_m^{ATP} of 90 μM (Fig. 2a). This leads to a k_{cat}/K_m value of 7.4 mM^{-1} min^{-1}, an enzymatic efficiency comparable with previously reported DDX1 data, although the underlying k_{cat} and K_m values are very different (Table 1). While both ATP hydrolysis efficiencies are within previously published ranges for other DEAD-box helicases, the values are 5- to 10-fold lower than published results for DDX3 (Table 1) [13,35].

To evaluate the role of RNA in DDX21 ATPase activity, ATP hydrolysis was tested as a function of RRE stem IIB concentration in the presence of saturating ATP, resulting in a k_{max}^{IIB} of 0.75 min^{-1} and a K_{app}^{IIB} of 0.85 μM (Fig. 2b, Table 1). DDX21's relative enzymatic specificity (k_{max}/K_{app}^{IIB}) of 0.88 represents a ~36-fold decrease when compared to DDX1 in the presence of stem IIB (Table 1) [13]. Previous DDX3 and DDX21 ATP hydrolysis studies utilized a poly-U RNA substrate with both high specificity and efficiency [35]. DDX21 ATPase assays were repeated using a similar poly-$(U)_{20}$ reagent and resulted in k_{max} and $K_{app}^{(U)20}$ values of 1.08 min^{-1} and 0.20 μM, respectively (Table 1), or a ~7-fold increase in $k_{max}/K_{app}^{(U)20}$ substrate specificity when compared to stem IIB. This may be a result of either a preference of DDX21 for the single-stranded nature of the poly-U sequence over a highly base-paired RRE stem IIB or a sequence preference for uridines. While there is a difference in substrate specificity, both RNA substrates efficiently stimulate ATPase activity at levels comparable to those reported for other DEAD-box helicases [13,37,38].

DDX21 helicase is stimulated by, but not dependent on, ATP

While RNA-stimulated ATPase activity is often described as a byproduct of DEAD-box helicase activity, it does not directly assess the ability of an enzyme to dissociate base-paired nucleotides. To determine the helicase activity of DDX21, a recently developed fluorescence-based unwinding assay was adapted [39]. Briefly, a fluorescein-labeled 10mer RNA is hybridized to an RNA 26mer labeled with a dabcyl quencher, designed so that duplex formation results in quenching of the fluorescent signal. The unwinding activity is measured in the presence of an excess of unlabeled competitor 14mer RNA, where strand separation results in irreversible dissociation of

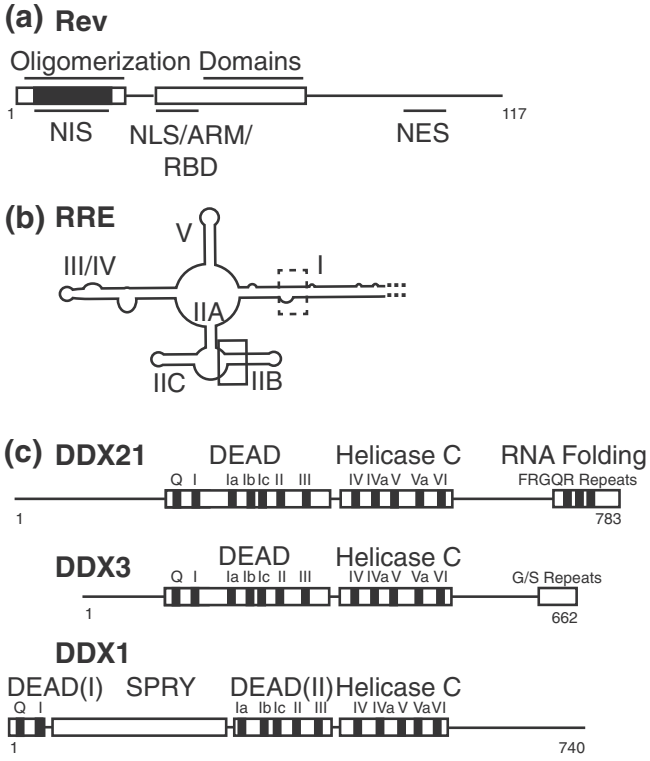

Fig. 1. Schematic diagrams of proteins and RNA used in this study. (a) Rev, with structured helix-turn helix domains boxed. Oligomerization domains, nuclear export inhibitory signal (NIS, nuclear localization signal (NLS, arginine-rich motif (ARM), RNA-binding domain (RBD), and nuclear export signal (NES) labeled. NIS region has additionally been colored black. (b) RRE RNA molecule, with stems I, IIA, IIB, IIC, III/IV, and V labeled. High-affinity primary binding site boxed in black, and lower-affinity binding site boxed in dotted line. (c) DDX21, DDX3, and DDX1 diagrams aligned to DEAD domain and helicase C domain interface. Accessory domains are labeled.

the quencher modified RNA, and an increase in overall sample fluorescence (Fig. 3a).

In the absence of DDX21 protein and ATP, there is little increase in fluorescence intensity over time, indicating a stable RNA hybrid (Fig. 3b). In the presence of DDX21, and the absence of exogenous ATP, fluorescent signal increases over time, with an unwinding rate constant (k_{unw}) of 0.11 ± 0.01 min^{-1}. It is possible that ATP was co-purified with the DDX21 protein, acting as the energy source for the observed "ATP-independent" helicase activity. This seems unlikely due to the fact that the amount of ATP that would be co-purified would be hydrolyzed quickly at the given RNA and protein concentrations. Another explanation would be contaminating RNase activity, but this also seems unlikely since the protein can be used in RNA-binding assays (see below). Therefore, DDX21 exhibits a basal helicase activity that does not require the hydrolysis of excess ATP. When ATP is added to the DDX21 helicase assay, k_{unw} increases 3-fold to 0.37 ± 0.01 min^{-1}. These data together indicate that while exogenous ATP may not be required, it does enhance RNA strand separation rates by DDX21.

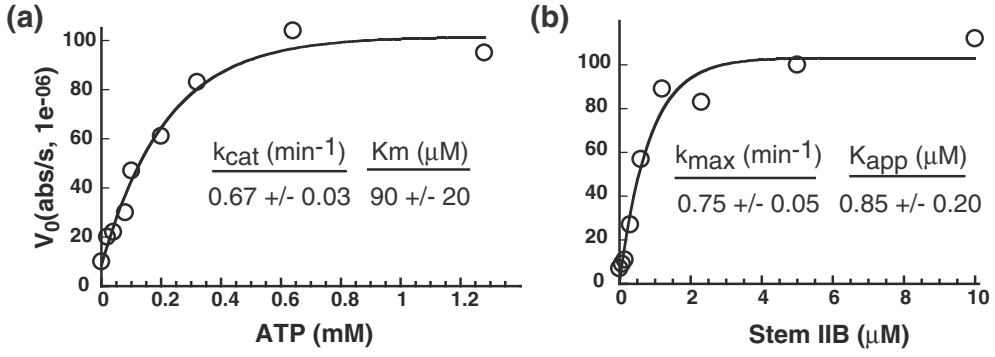

Fig. 2. DDX21 ATPase activity is RNA dependent. (a) Spectroscopic ATPase activity of DDX21 in the presence of 5 μM stem IIB RNA measured as a function of ATP concentration. K_{cat} and K_m values noted. (b) Increasing concentrations of stem IIB RNA were titrated into DDX21 in the presence of 2.5 mM ATP, with k_{max}^{IIB} and K_{app}^{IIB} values noted.

Table 1. Steady-state ATPase kinetics of DDX21a**

ATP titration (in the presence of excess RNA)

Construct	k_{cat} (min^{-1})	K_m (ATP) (mM)	k_{cat}/K_m (min^{-1} mM^{-1})
DDX21	0.67 ± 0.03	0.09 ± 0.2	7.4
DDX3[a]	3.2 ± 0.1	0.045 ± 0.003	71.1
DDX1[b]	15.2 ± 0.6	1.0 ± 0.1	15.2

RNA titration (in the presence of excess ATP)

Construct	RNA	k_{max} (min^{-1})	K_{app} (RNA) (μM)	k_{max}/K_{app} (min^{-1} μM^{-1})
DDX21	IIB	0.75 ± 0.05	0.85 ± 0.2	0.9
	Poly $(U)_{20}$	1.08 ± 0.05	0.20 ± 0.04	5.4
DDX1[b]	IIB	16.0 ± 0.4	0.50 ± 0.05	32.0
	RRE	16.8 ± 0.6	0.24 ± 0.05	70.0
	tRNA	13.5 ± 0.6	1.9 ± 0.3	7.1
	RRE + 1× Rev	17 ± 1	0.2 ± 0.1	85.0
	RRE + 2× Rev	16 ± 1	0.3 ± 0.2	53.0
	RRE + 4× Rev	13.5 ± 0.6	1.9 ± 0.3	7.1

[a] Data from Garbelli *et al.* [35].
[b] Data from Edgcomb *et al.* [13].

Rev inhibition of ATPase-related activities is due to RNA binding

DDX1 RNA-dependent ATPase activity is inhibited by the presence of Rev in a dose-dependent manner (Table 1) [13]. Similarly, DDX21 shows a dose-dependent ATPase inhibition by Rev when using a stem IIB concentration of 3.3 μM and excess ATP (Fig. 4). This decrease in activity could be due to Rev sequestering ATP from DDX21, sequestering RNA from DDX21, or directly inhibiting DDX21 activity through a protein–protein interaction. ATP hydrolysis assays were repeated in the presence of 1.65 μM stem IIB RNA to test the effects of RNA concentration on Rev-dependent inhibition, and indeed, it inhibited DDX21 ATPase activity more efficiently at lower RNA concentrations (Fig. 4a). Furthermore, this inhibition was markedly relieved when an RNA-binding-defective Rev mutant, Rev N40A, was introduced instead of WT Rev (Fig. 4a). These data together would indicate that Rev-dependent inhibition of DDX21 activity is closely related to Rev's ability to bind the RNA substrates, either titrating away the effective RNA reaction pools or by directly inhibiting DDX21 activity in an RNA-bound form.

RNA helicase assays were performed using increasing concentrations of Rev to better understand the inhibition in DDX21-related enzymatic activities (Fig. 4b, Table 2). In the presence of excess ATP, RNA helicase rates decreased when Rev was added in a dose-dependent manner. Although this effect mirrors those observed with ATPase assays above, it is important to note that non-zero helicase activity remains at the end point of the titration. Indeed, DDX21 helicase activity levels out to rates seen for helicase assays performed in the absence of ATP (Fig. 4b, Table 2). When the same experiment is performed in the absence of ATP, there is little change in the basal helicase activity, indicating that Rev-dependent inhibition is somehow associated with ATP-dependent helicase activity only (Fig. 4b, Table 2). This is somewhat surprising given that the same RNA substrate is used for both ATP-dependent and ATP-independent activities. If Rev binding to the RNA substrate was inhibiting binding to DDX21, it would be expected that both ATP-dependent and ATP-independent activities are inhibited, which they clearly are not. This would indicate that the mechanism of inhibition is more complicated than titration of the RNA substrate from the active reaction pool by Rev, although it is unclear what that mechanism might be.

DDX21 interacts with Rev at low nM affinity directly through a conserved DEAD domain

Previous binding studies between DDX1 and Rev demonstrated a direct and high-affinity interaction, with a dissociation constant of ~40 nM (Table 3) [13,24]. Furthermore, the binding site of DDX1 was mapped to the highly conserved DEAD domain of DDX1 and not the SPRY domain, as previously suggested (Table 3) [24]. This led to the hypothesis that Rev interacts with DEAD-box proteins in a conserved manner. To assess this, previously established fluorescence binding assays were conducted between either DDX21 or DDX3 and fluorescently labeled Rev [13]. DDX21 binds to Rev with a dissociation constant (K_d) of 21 ± 7 nM, a value similar to DDX1, while DDX3 binds with a K_d of 122 ± 15 nM (Fig. 5a, Table 3). The DEAD domains of DDX3 and DDX21 were independently tested for binding to Rev, with near-WT binding dissociation constants of 60 ± 9 and 200 ± 83 nM, respectively (Table 3). Therefore, the DEAD domain of each DEAD-box protein is sufficient for high-affinity binding to Rev, again suggesting a conserved

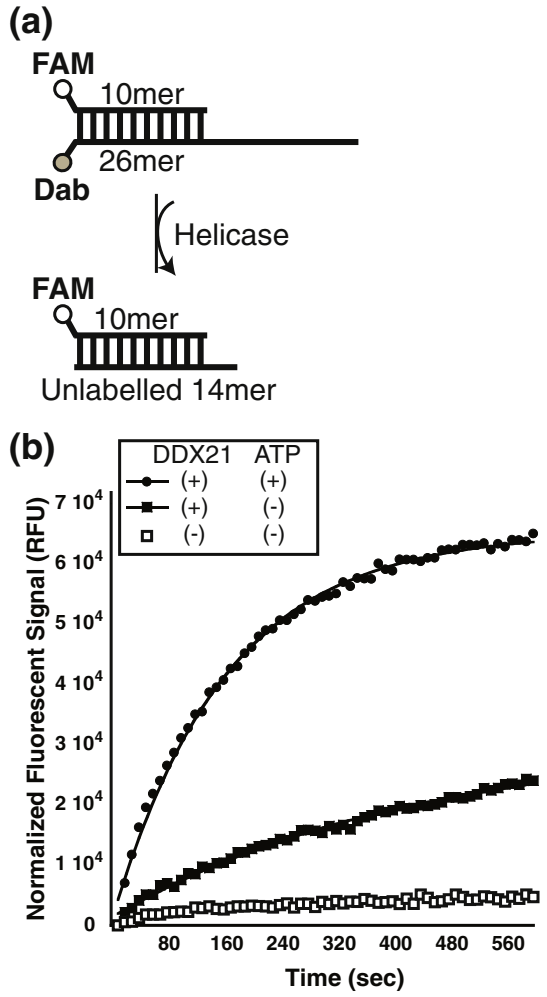

Fig. 3. DDX21 helicase activity is stimulated by ATP. (a) Schematic diagram of RNA molecules used in helicase assay. A fluorescently labeled RNA 10mer is annealed to a fluorescent quencher 26mer. Once the strands separate, the 10mer reanneals to the excess unlabeled 14mer, resulting in a fluorescent signal. (b) Helicase assay results showing a graph of fluorescent intensity over time for RNA dimer alone (open boxes), DDX21 with RNA dimer (closed boxes), and DDX21 with ATP and RNA dimer (closed circles).

mechanism of binding between this family of proteins and Rev.

Rev interaction with DDX21 is affected by 4 aa located within the nuclear diffusion inhibitory signal

Work by Fang *et al.* [15,40] demonstrated that a segment of Rev, the nuclear diffusion inhibitory signal (NIS), was sufficient to interact with DDX1 *in vivo* (diagramed in Figs. 1c and 5d). Furthermore, mutations made in this region disrupt Rev–DDX1 interaction *in vivo* [13] and *in vitro* (Table 4). Because this region is also required for higher-order Rev multimerization, mutations that inhibit Rev–DDX interaction have been shown to also inhibit Rev–Rev interaction [2,9,41]. This has led to two possible models to explain binding defects of these mutants. Either the NIS region is directly responsible for binding to DDX proteins or DDX proteins may require Rev dimerization to bind.

To distinguish which of these models is operative, a previously identified monomer-only Rev mutant, SLT40, was tested for binding to DDX21 [42]. Here residues I59 and L60, positions located in one part of the Rev oligomerization domains but outside the NIS, have been mutated to aspartic acids, leading to a defect in higher-order Rev oligomerization (Fig. 5b). Rev-SLT40 binds to DDX21 at near-WT affinity (K_d of 49 ± 17) (Fig. 5c, Table 4), which is consistent with a binding model where monomeric Rev binds to DDX21, with the Rev NIS acting as a DDX binding platform.

To further characterize the interaction between DDX21 and Rev, a single alanine scan of the monomeric SLT40 Rev NIS was performed (Table 4). While most alanine position mutations showed small to no binding defect, four positions, L13, K14, V16, and L18, showed substantial and reproducible defects. Of these, K14A displayed the largest binding defect with a decrease in binding affinity of greater than 100-fold (Fig. 5c and d and Table 4). These data taken together strongly implicate the NIS region in direct binding to DDX21, and by extension, to other DDX proteins.

DDX protein interaction profile with Rev *in vivo*

Multiple studies have investigated the interaction of DEAD proteins and RCCs *in vivo* [10,12,13,20–22]. For example, one study demonstrated that DDX21 or DDX3 interact with RCCs *in vivo* and suggested that this interaction was differentially RNA dependent [10]. In another series of experiments, DDX1 interaction with RCCs was shown to be disrupted by a V16D mutation [13]. To more clearly compare the interactions of all three DEAD-Box proteins with RCCs and the importance of RNA in this interaction, co-IP experiments were performed.

For this work, a stable HeLa cell line containing a chromosomally integrated doxycycline-inducible Gag-RRE expression construct, termed T-Rex-GagRRE HeLa, was established (Fig. 6a). These cells were transduced with a lentiviral vector encoding Rev-GFP-V5. In some cases, cells were co-transduced with vectors encoding either DDX1 or DDX21 to increase intracellular concentrations of these helicases; endogenous levels of DDX3 were deemed sufficient for this work. The expression of the GagRRE mRNA was induced in the various cell populations with doxycycline, and cells were then harvested. IPs then were performed using antibodies against DDX21, DDX1,

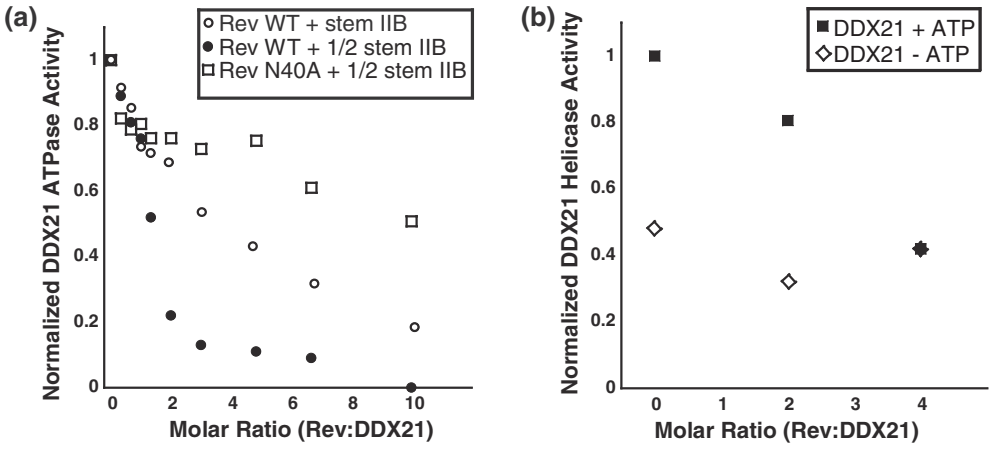

Fig. 4. Rev inhibits DDX21 ATP hydrolysis and ATP-dependent helicase activities. (a) Relative DDX21 ATP hydrolysis activity in the presence of 2 μM stem IIB and WT Rev (open circles), 1 μM stem IIB and WT Rev (closed circles), and 1 μM stem IIB and Rev N40A. (b) Relative DDX21 RNA unwinding activity in the presence (closed boxes) and absence (open diamonds) of 2.5 mM ATP.

and DDX3, and Western blotting was performed to assess helicase IP efficiency and co-IP of Rev.

Each DDX-specific antibody efficiently immunoprecipitated its cognate target protein (Fig. 6b). When samples were probed for the presence of Rev, all DDX-specific antibodies showed significantly higher co-IP signal than with the negative control mouse IgG (Fig. 6b). To assess the role of RNA in the DDX/RCC interactions, some samples were incubated with RNase A prior to IP (Fig. 6b). For DDX21 and DDX1, the co-immunoprecipitated Rev levels decreased when compared to RNAse untreated samples but were still clearly detected. Co-IP of Rev was not detected for DDX3 in the presence of RNAse A. To further investigate the role of direct protein binding on RCC/DDX association, Rev V16D was tested for the ability to associate with each DDX protein complex. In each case, Rev showed an absence or marked decrease in IP with DEAD-box proteins, as would be expected if *in vivo* association were due to a direct interaction (Fig. 6b, fourth row of panels).

These data indicate that these three tested DEAD-box proteins can robustly interact with RCCs *in vivo*, and while RNA may enhance this interaction, it does not seem strictly required for DDX1 and DDX21 binding. Furthermore, mutations that inhibit the interaction between DDX proteins and Rev *in vitro* also inhibit the interaction between DDX proteins and RCCs *in vivo.*

DDX21 binds more tightly to the RRE than to DDX1

We previously demonstrated that DDX1 interacts with the full-length RRE with an apparent K_d of ~250 nM using electrophoretic gel shift assays (EMSAs) and radiolabeled RNA [13]. Furthermore, when these assays were conducted at higher current, the RNA–protein complex dissociated,

Table 2. RNA helicase unwinding constants for DDX21

DDX21 construct	ATP	k_{unw} (min^{-1})
(–)	(–)	—
WT	(–)	0.11 ± 0.01
WT	(+)	0.37 ± 0.01
(183–620)	(–)	—
(183–620)	(+)	0.29 ± 0.01
Rev titration		
WT + 0 Rev	(+)	0.31 ± 0.01
WT + 2× Rev	(+)	0.25 ± 0.01
WT + 4× Rev	(+)	0.13 ± 0.01
WT + 0 Rev	(–)	0.15 ± 0.01
WT + 2× Rev	(–)	0.10 ± 0.01
WT + 4× Rev	(–)	0.13 ± 0.01

Table 3. DDX protein equilibrium dissociation constants for Rev WT

DEAD-box protein	K_d (nM)
DDX21	21 ± 7
DDX21 DEAD	60 ± 9
DDX21(183–620)	48 ± 27
DDX3	122 ± 15
DDX3 DEAD	200 ± 83
DDX1	41 ± 11
DDX1 DEAD[a]	79 ± 7
DDX1 SPRY[a]	n.d.

[a] Data from Hammond *et al.* [24].

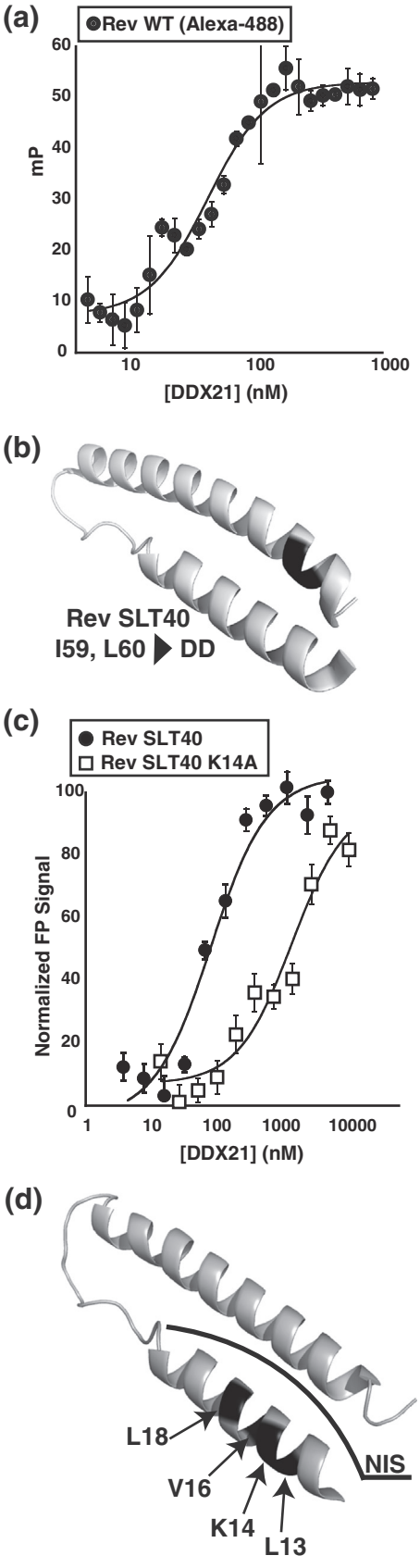

Table 4. Protein equilibrium dissociation constants for Rev and mutants

Rev Construct	K_d (nM)
DDX21 bound	
Rev WT	21 ± 7
Rev SLT40	49 ± 17
Rev SLT40 E10A	29 ± 17
Rev SLT40 D11A	42 ± 19
Rev SLT40 L12A	240 ± 23
Rev SLT40 L13A	>1110
Rev SLT40 K14A	>2714
Rev SLT40 V16A	>1119
Rev SLT40 V16D	>1225
Rev SLT40 R17A	89 ± 55
Rev SLT40 L18A	>630
Rev SLT40 I19A	315 ± 250
Rev SLT40 K20A	79 ± 19
Rev SLT40 F21A	210 ± 154
Rev SLT40 L22A	297 ± 258
Rev SLT40 Y23A	38 ± 30
Rev SLT40 Q24A	54 ± 30
DDX1 bound	
Rev WT	41 ± 11
Rev V16D	>500

revealing a DDX1-dependent RRE structural transition [24]. To test the apparent RNA-binding affinity of DDX21, EMSA experiments were again performed under high current conditions. As seen with DDX1, DDX21 binding resulted in the RNA signal shifting to the well (Fig. 7a). However, DDX21 bound to the RRE RNA with 5- to 10-fold higher affinity when compared to DDX1 (apparent K_d of 37 ± 2 nM). Furthermore, no additional DDX21-dependent RNA species were resolved under high-current conditions.

Because DDX21 association results in a "well-shift" in radioactive EMSA assays, a DDX21 construct was created composed of the conserved DEAD and helicase C domains required for ATP-dependent helicase activity in DDX proteins, as well as preserving the conserved Rev binding site. The construct, labeled DDX21(183–620), shows an efficient ATP stimulation of helicase activity, although the residual ATP-independent helicase activity was no longer present (Table 2). DDX21(183–620) resolves into distinct protein-bound RRE species when using a previously described modified EMSA assay where the RNA is visualized *via* UV fluorescence (Fig. 6b, middle panel) [43]. Upon the addition of Rev, previously described

Fig. 5. DDX proteins bind to Rev in a similar manner. (a) A representative fluorescence polarization experiment with fluorescently labeled Rev and increasing concentrations of DDX21. For line fit, see Materials and Methods. (b) Tertiary structure of Rev (pdb: 4PMI) with SLT40 mutations (I59D, I60D) colored black. (c) Fluorescence binding data for Rev SLT40 and Rev SLT40 K14A). (d) Tertiary structure of Rev (pdb: 4PMI) with residues 13, 14, 16, and 18 labeled and colored black. NIS region is marked by a black line.

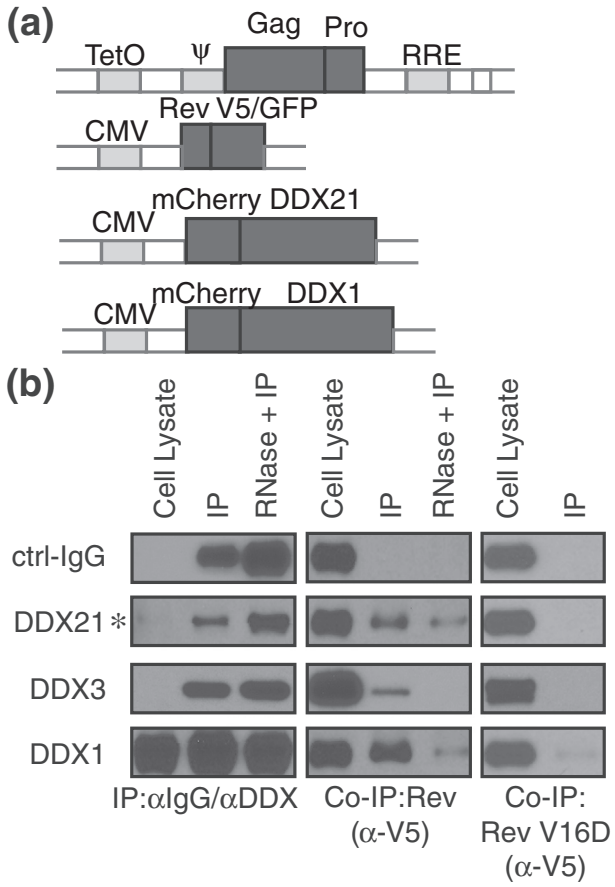

Fig. 6. Co-IP between Rev and DEAD proteins. (a) Schematic diagrams of the plasmids used for cell line engineering and lentivirus production. Top: plasmid for Flp recombinase-mediated integration and its expression is under the control of a CMV/Tetracycline-regulated promoter. Flp-In T-Rex HeLa cells were transfected with this plasmid and selected with hygromycin to establish stable T-Rex-GagRRE HeLa cells. The bottom three diagrams represent the lentivectors containing indicated proteins. (b) Western blot analysis of co-IP between Rev and DEAD proteins. To examine the interactions of DEAD helicases and Rev, T-Rex-GagRRE HeLa cells were transduced with lentiviruses of Rev-GFP-V5 for DDX3 IP, or co-transduced with lentiviruses of mCherry-DDX1-V5 or mCherry-DDX21-V5 for 24 h, followed by doxycycline addition for another 24 h for DDX1 or DDX21 IP. Cell lysates with and without RNase treatment were incubated with indicated antibodies and then analyzed by Western blotting, as indicated. Cells expressing Rev(V16D)-GFP-V5 were analyzed with Rev-GFP-V5 in parallel. Asterisk indicates overexposed samples for better visualization.

single-step oligomeric RRE/Rev species can be resolved (Fig. 7b, top panel). A similar titration of DDX21(183–620) results in the formation of two distinct species at lower concentrations and a third at higher concentrations (Fig. 7b, middle panel).

To test the ability of Rev, DDX21(183–620) and the RRE to form a tripartite complex, an EMSA was

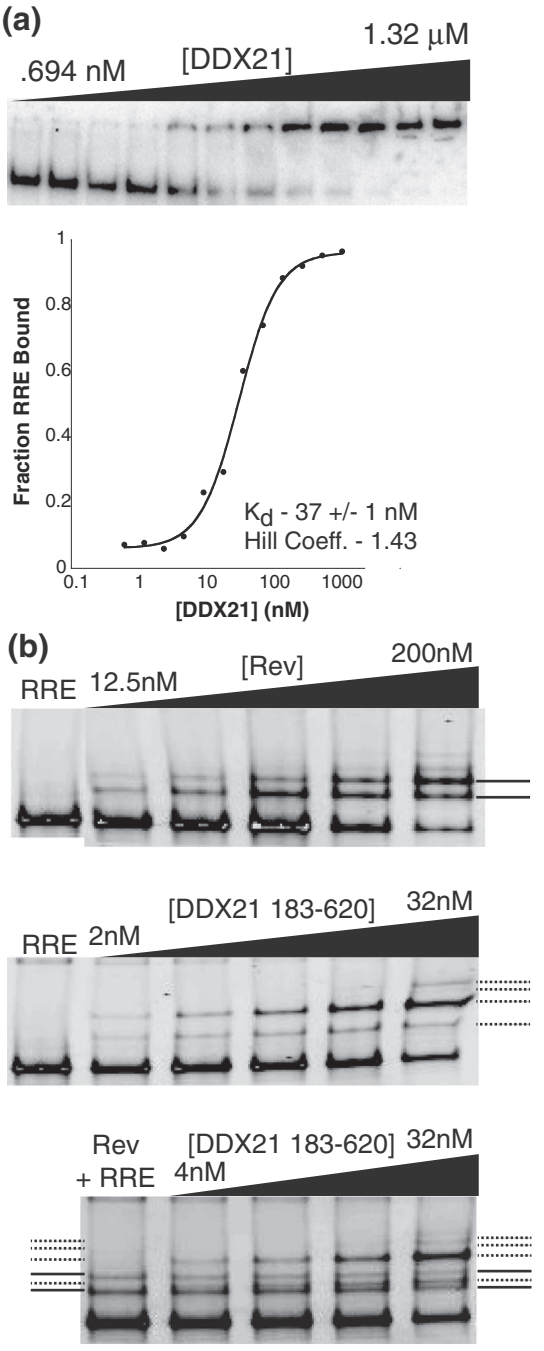

Fig. 7. DDX21 and Rev bind independently to the RRE. (a) Electrophoretic gel mobility shift titration of DDX21 into radiolabeled RRE RNA (top panel) and quantified fraction-bound graph (on bottom). See Materials and Methods for line fit of bottom panel. K_d is noted on bottom. (b) EMSA titration of Rev (top panel), DDX21(183–620) (middle panel), and DDX21(183–620) in the presence of 25 nM Rev (bottom panel) into RRE RNA; RRE band imaged *via* ethidium bromide staining and UV fluorescence. Rev-dependent species are marked by a solid line; and DDX21(183–620)-dependent RNA species, by dotted lines.

performed with constant concentrations of Rev and RRE and increasing concentrations of DDX21(183–620). Surprisingly, instead of the predicted formation of a three-member complex, only a combination of the previously described species was observed (Fig. 7b, bottom panel). This would indicate that the tripartite species concentration is so small it cannot be imaged using this technique, or the complex is too unstable for evaluation using EMSAs, or that a ternary complex does not form.

DDX21 enhances Rev oligomerization on the RRE in parallel to DDX1

A hallmark of the Rev/RRE assembly pathway is the initial high-affinity binding of a single Rev protein to stem IIB and subsequent oligomerization of Rev along the RRE utilizing both RNA and protein binding domains [2,3,9,44,45]. EMSA experiments have been used historically to discern the number of Rev monomers bound to the RRE at any given concentration [3,45]. However, our previous work demonstrated that these data are actually a convolution of both RRE structural transitions and Rev binding events [24]. Therefore, only an assay that directly measures the binding of Rev to the RRE can be used to assess effects of DDX proteins on Rev binding and subsequent oligomerization on the RRE. One such method uses total internal reflection fluorescence (TIRF) microscopy to visualize Rev association with the RRE at single-molecule resolution [14,23,24,46]. In this experiment, a full-length RRE molecule is immobilized on a quartz surface *via* biotin–streptavidin attachment, utilizing a biotinylated oligonucleotide that is hybridized at the 3′ end of the RRE. Then, Rev labeled at a specific cysteine residue with Alexa Fluor 555 (A555) is allowed to interact with the RRE and is excited through the evanescent field of a 532 nm laser. A representative fluorescence intensity *versus* time trace showing Rev molecules interacting with a single immobilized RRE molecule is presented in Fig. 8a. Rev associates with and dissociates from the RRE several times during the observation period (Fig. 8a). A single Rev monomer emits a fluorescent intensity of ~200 a.u. in our experimental conditions, so one RRE-bound Rev molecule has an intensity of 200 a.u.

A histogram of all binding events in each experiment can be compiled and the distribution of Rev oligomerization states can be assessed (Fig. 8c, top left panel). At the concentrations used in this experiment (1 nM Rev), Rev binds to the RRE primarily as a monomer (a dominant signal at 200 a.u.), with a minor peak corresponding to two bound Rev monomers. As demonstrated previously, the presence of DDX1 increases the proportion of fluorescent signal at higher-intensity values, indicating an increase in the number of Rev monomers associated with each RRE molecule (Fig. 8c, bottom right panel) [46]. Recently, we showed that DDX1 acts through the RRE RNA to promote Rev–RRE assembly [23,24]. This ability of DDX1 to promote oligomerization of Rev on the RRE may be a general property shared by other DEAD-box helicases, or this activity might reflect the helicase activities and substrate preferences of a particular helicase. Indeed, when DDX21 was added to a Rev/RRE assembly assay, enhanced oligomerization behavior of Rev was again observed, similar to that in the presence of DDX1 (Fig. 8b and c, top right panel). Surprisingly, the presence of DDX3 had little effect on Rev oligomerization on the RRE (Fig. 8c, bottom left). This indicates that DDX3 does not promote Rev oligomerization on the RRE as efficiently as DDX1 or DDX21.

We also performed a dwell time analysis for the first Rev monomer binding to the RRE in the presence of DDX21 or DDX1. In both cases, we observed similar bi-exponential kinetic behavior: rate constants of 1.06 ± 0.20 and 0.16 ± 0.06 s^{-1} in the presence of DDX21 (Fig. 8d, left) and 1.38 ± 0.18 and 0.11 ± 0.02 s^{-1} in the presence of DDX1 (Fig. 8d, right). In both cases, the fast phase is predominant, whereas the slow phase corresponds to the Rev binding rate observed in the absence of any DDX protein (0.09 ± 0.01 s^{-1}), agreeing with previous results [23]. These results indicate that DDX1 and DDX21 both accelerate binding of the first Rev monomer to the RRE and likely act by a similar mechanism.

Discussion

DDX21 is a multifunctional enzyme

DEAD-box helicases are multifunctional proteins that can directly bind to RNA and nucleoside triphosphates through their DEAD-box homology domains and bind to additional factors through accessory domains [47]. DDX21, a protein first isolated from Hela cell nuclear extracts, was characterized previously, exhibiting ATPase/dATPase and RNA unwinding activities [48]. Here we characterized the recombinant, untagged DDX21 protein, focusing on RNA-stimulated ATPase activity, RNA helicase activity, and direct RNA and accessory protein binding. Fig. 9 diagrams a summary of the binding and enzymatic activities of DDX21 in this work, as well as indicating hypothetical activities hinted by our research. These data indicate that the measured ATPase and helicase enzymatic activities of DDX21, like DDX1 and DDX3, fall within the range of activities generally observed for DEAD-box helicases. Surprisingly, even in the absence of ATP, some basal helicase activity was observed for DDX21. It is unclear what the mechanism of an ATP-independent helicase activity might be, or indeed if it has a physiological relevance outside this artificial context, but it is worth

noting that this activity was not present in the DEAD-core DDX21(183–620), although ~80% of the ATP-dependent helicase activity of the full-length enzyme was retained (Table 2). This might indicate a synergistic activity between the DEAD core and accessory domains during RNA remodeling.

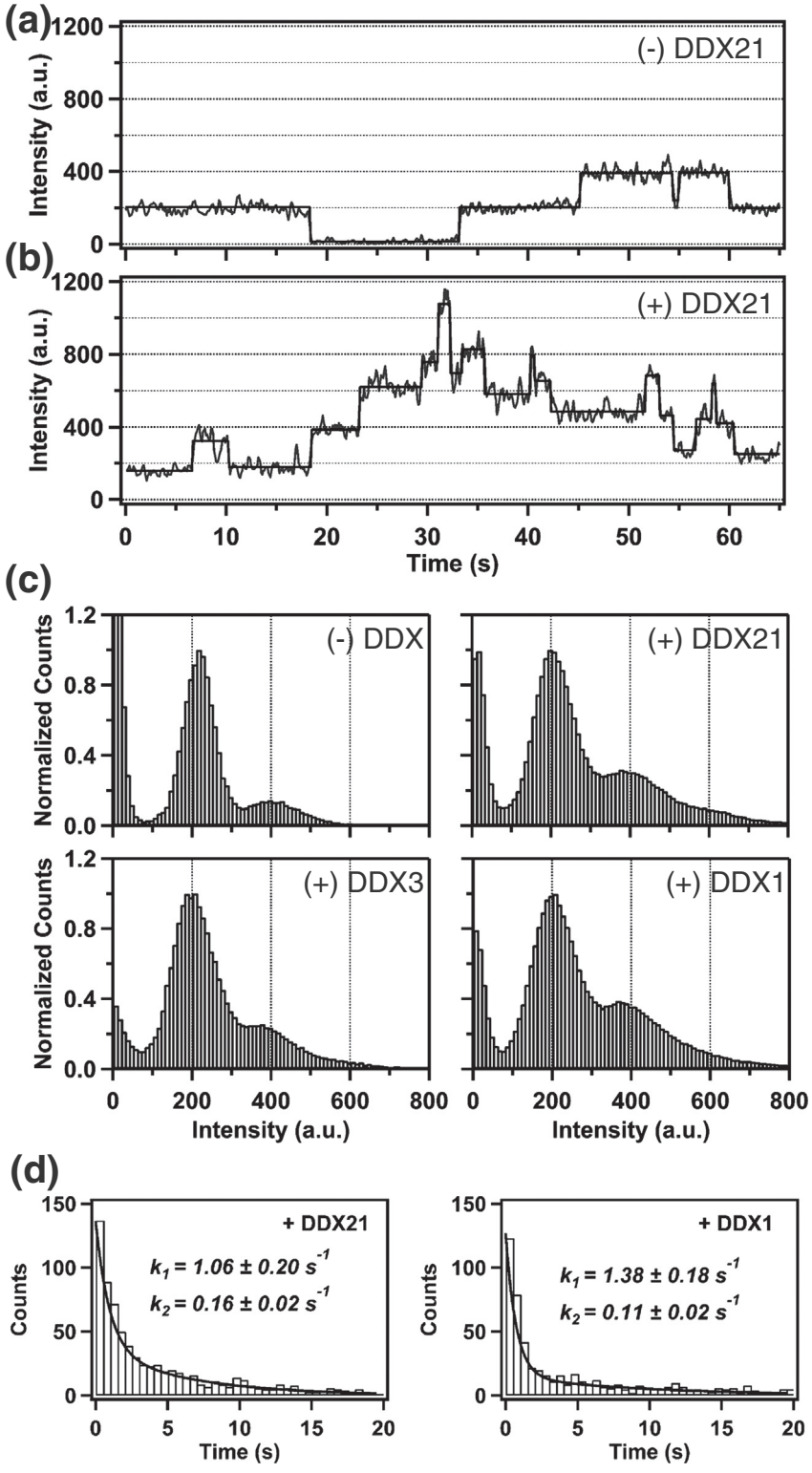

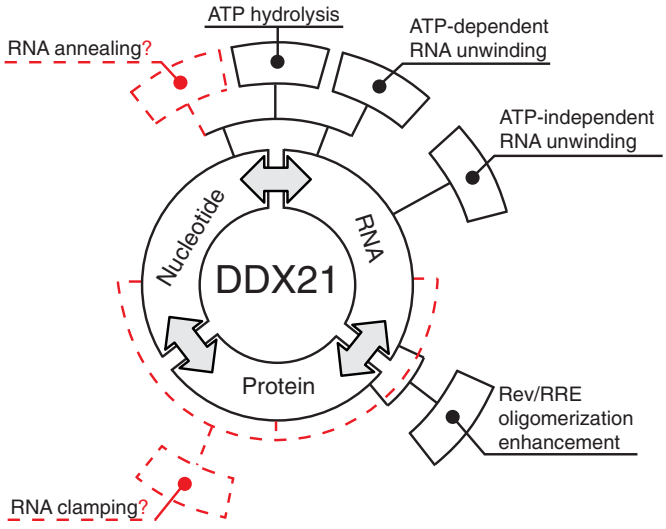

Fig. 9. Binding and enzymatic activities of DDX21. DDX21 enzyme has RNA, nucleotide, and protein binding activities (first level of boxes in black). One binding activity is often affected by other binding activities (annotated by double-headed arrows) and can combine to create enzymatic effects (annotated by boxes in the second layer). Often, multiple binding activities are required for single enzymatic activities (solid and dashed lines from first to second tiers). Solid black boxes in the second ring are enzymatic or functional activities measured in this study, while dashed red boxes represent activities only suggested by this or other studies. Figure adapted from Putnam and Jankowsky [47].

DDX21 and the Rev/RRE components

The Rev binding activities of DDX21, DDX3, and DDX1 are strikingly similar. Each was previously shown to interact with RCCs *in vivo* [10,13,15,40], and work here has demonstrated the ability of each of these proteins to interact directly with Rev through their respective DEAD domains. This conserved mode of binding would likely explain why Rev is able to interact intracellularly with a large number of DEAD-box proteins [10,20]. The data presented here indicate a direct role for the Rev NIS in this protein–protein interaction. Of the residues shown to have an effect on binding, only L13 and V16 show high conservation among HIV strains, while position 14 shows a high preference for basic amino acids and position 18 for nonpolar amino acids [45]. Furthermore, the V16D mutations in Rev result in a binding defect in both DDX21 and DDX1 *in vitro* and *in vivo,* implicating a direct protein–protein interaction between Rev and DEAD-box proteins intracellularly.

DDX21 binds to the RRE with a higher affinity than that reported for DDX1. However, ATPase assays suggest that RRE-derived RNAs are not better substrates for activity than generic oligoribonucleotides, indicating that while the RRE is itself a substrate for RNA-dependent ATPase activity, it is not necessarily a preferred one.

Titration of excess Rev protein into DDX21 ATPase and RNA unwinding assays showed a dose-dependent inhibition of DDX21 activity (Table 2, Fig. 4). This inhibition is not significant in the presence of stoichiometric amount of Rev protein, and supplying excess RNA reduces the apparent inhibition, as does the addition of an RNA-binding-defective mutant of Rev. On the basis of the observations above, we propose that both ATPase and ATP-dependent RNA unwinding activities of DDX21 are inhibited by Rev, and this inhibition is linked to Rev's RNA-binding properties. A possible explanation would be that Rev, at the concentrations used here, titrates RNA substrates away from DDX21 binding. However, data indicating

Fig. 8. Assembly of Rev on the RRE monitored by single-molecule fluorescence spectroscopy. (a) Rev–RRE assembly in the absence of any DDX protein. Representative time trace (gray) of A555 emission over time, showing individual Rev monomer binding and dissociation events. The emission intensity of a single Rev monomer is ~200 units. The black lines are fits to a hidden Markov model. (b) Rev–RRE assembly in the presence of 150 nM DDX21. Same format as in panel a. More Rev monomers assemble on the RRE in the presence of DDX21. (c) Normalized intensity histograms compiled from more than 100 traces, representing individual Rev–RRE stoichiometry states as separate peaks in the absence and presence of 150 nM DDX proteins, as indicated. (d) Dwell time histograms for the first Rev monomer binding to the RRE in the presence of DDX21 (left) and DDX1 (right). Histograms were fitted to a bi-exponential function, indicated by the solid line. The fitted rate constants and their associated uncertainties are indicated.

that DDX21's ATP-independent RNA helicase activity is not affected by Rev would suggest a mechanism more complicated than simple titration. Indeed, the data presented here would be consistent with an RNA clamping model, where hydrolysis byproducts are not released, but some background helicase activity is observed due to stable DDX/RNA binding and induction of strand displacement in the presence of Rev [49]. However, it seems unlikely that the *in vivo* concentration of Rev would be high enough for total nuclear DDX21 population ATPase inhibition [50,51].

DDX1 and DDX21 have similar activities

Our results indicate that DDX1 and DDX21 (and unlike DDX3) have very similar biochemical properties, binding to Rev with similar affinities through their conserved DEAD domains, reorganizing RNA architecture in the absence of ATP and enhancing Rev oligomerization on the RRE. Previous work *in vivo* indicated that while these proteins may have similar roles in the HIV life cycle, they are not merely redundant members of an export mechanism, as the knockdown of either has a significant effect on HIV release from the cell, although they may be involved in the same mechanism [10,13]. These overlaps in function may reflect a direct interaction between DDX1 and DDX21 in the cell, and indeed, these proteins have been implicated as playing a part in the double-stranded RNA pathway together and were hypothesized to directly interact with each other to do so [31]. Future studies investigating the role each of these proteins play in the RRE export process, as well as their native cellular interaction and functions together, are a natural extension of the present work.

DDX21, DDX1, and DDX3 in the Rev/RRE assembly pathway

We previously hypothesized that all that would be required for the stimulation of Rev binding to the RRE is a functionally conserved DEAD-helicase protein capable of binding RNA (as demonstrated for DDX1) [24]. To test this, Rev oligomerization assays were performed using TIRF microscopy and indicated that DDX1 and DDX21 had nearly identical effects on both Rev oligomerization and Rev's initial RRE on-rate. Somewhat surprising was the relative lack of effect DDX3 had in this assay. These data taken with *in vivo* IP experiments presented here, as well as from other papers, would indicate that while DDX3 is capable of interacting with RCCs *in vivo*, its mechanistic role is distinct from that of DDX1 and DDX21 [10,16–19,21,22]. Indeed, DDX3 is somewhat unique in that it is capable of efficiently interacting with a variety of nucleic acid partners, including NTPs, dNTPs, DNA, and RNA [35]. This broad specificity likely reflects its previously implied roles in HIV translation and nuclear pore export, but unfortunately, it does not explain the mechanistic role it might be playing in Rev-related processes.

It remains unclear what roles DEAD-box proteins play in the HIV life cycle. This is partly due to the fact that their mechanistic roles in native cellular processes are still not well understood, and the authentic substrates for the HIV-specific functions for helicases are not yet defined. HIV represents a somewhat simplified platform with which to understand the enzymatic and functional roles these helicases perform *in vivo*, and in this work, we more clearly define the biochemical activities of DDX21, DDX1, and DDX3. However, while we have RNA, nucleotide, and protein binding data for these three DDXs, the critical step to connect these activities with specific steps in the HIV life cycle remains unclear. Our work here and previously now provides a number of tools to study the role of DEAD-box helicases in the Rev/RRE pathway *in vivo* and the HIV life cycle.

Materials and Methods

Plasmid construction for protein purification

RRE, DDX1, and Rev S10C constructs are described previously [14,24,41]. Rev_{SLT40} and subsequent alanine mutants described above were created using Quick Change II site directed mutagenesis (Agilent) according to manufacturer protocol. DDX3, DDX21, and subdomain constructs were created using Gateway Cloning Technology™ (Invitrogen). DDX21 (HsCD00042538) and DDX3 (HsCD00040249) containing constructs in pDONR221 were purchased from DNASU. A DDX3 DEAD domain comprising aa 211–403, a DDX21 DEAD domain of aa 217–396, and DDX21(183–620) were PCR amplified and recombined into fresh pDONR221 according to the manufacturer's protocol (Invitrogen). All DDX proteins and subdomains were then recombined into pDest566 according to the manufacturer's protocol. Final plasmids were named pMBPDDX3, pMBPDDX3DEAD, pMBPDDX21, pMBPDDX21DEAD, and pMBPDD X21183–620. Each construct contained, from the N-terminus, coding regions for a 6X His-tag, an MBP tag, and a Tev cleavage site and ended in the DDX protein of interest. All plasmids were verified *via* sequencing reactions (Eurofins Operon). Gateway vectors were a generous gift of the Dominic Esposito Lab at the National Cancer Institute.

Plasmid construction for human cell *in vivo* protein expression

Rev WT, V16D, and EGFP were amplified by PCR and digested with NheI and XhoI, XhoI, and SacII, respectively. The digested fragments were then cloned into pcDNA3.1 (Invitogen) containing V5

epitope tag. The whole cassette of Rev-EGFP-V5 was then digested with NheI and PmeI, and ligated to lentiviral vector pCDHblast MCSNard OST-LMNA (with CMV promoter, a gift from Tom Misteli) (Addgene plasmid no. 22661) where OST-LMNA was removed by BamHI and NotI, then replaced with oligos containing NheI and BstZ17 I. Constructs containing DDX1 or DDX21 were amplified by PCR, digested with NheI and XhoI, and inserted into pcDNA3.1 containing mCherry and V5 tag at N-terminus and C-terminus of multiple cloning sites (unpublished), respectively. The cassettes of mCherry-DDX1-V5 or mCherry-DDX21-V5 were then amplified by PCR, digested with BamHI and SalI, and then cloned into lentiviral vector (with CMV promoter, a gift from Eric Campeau) (Addgene plasmid no. 17448).

Flp-In T-Rex-GagRRE HeLa cell production

GagRRE was amplified by PCR from pCMV-GagRRE [52], digested with EcoRV and AleI, and cloned into pcDNA5-FRT-TO-6xMS2 (unpublished) with AleI site to generate pcDNA-FRT-TO-GagRRE-6xMS2. This plasmid was co-transfected with pOG44 into Flp-In T-Rex HeLa cells (Invitrogen), a gift from Don Cleveland, and subsequently selected with hygromycin to establish a stable cell line per the manufacturer's instructions. Cells were maintained in Dulbecco's modified Eagle medium (Gibco), 10% tetracycline-free FCS (Clontech), 2 mM L-glutamine (Gibco), 100 U ml^{-1} penicillin, and 100 µg/ml streptomycin (Gibco) at 37 °C in 5% CO_2 incubator.

DDX and Rev protein purification

All DDX1 (including subdomain constructs) and Rev (including mutant constructs) proteins were purified as previously described [13,24]. DDX3, DDX21, and sub-domain proteins were expressed in Rosetta pLysS cells (Novagen, Cambridge, MA), grown in LB broth to an OD_{600} of 0.6 at 37 °C. Temperature was then adjusted to 25 °C and protein expression induced by the addition of 1 mM IPTG for 12–18 h. Cells were harvested by centrifugation and stored at −20 °C until ready for use, or immediately used in protein purification. Cell pellets were resuspended and lysed in B-Per reagent (Pierce Biotechnology, Waltham, MA) supplemented with lysozyme (0.1 mg/ml) at room temperature for 20 min. Cell debris was removed by centrifugation, and the resulting supernatant was adjusted to 0.5 M NaCl and polyethyleneimine (Sigma, St. Louis, MO) added to a final concentration of 0.025%. The sample was again centrifuged to remove precipitated nucleic acid, and the resulting supernatant was applied to HisTrap column (GE healthcare) using an AKTA FLPC (GE Healthcare). After washing the column with wash buffer [20 mM Tris (pH 7.8) and 0.5 M NaCl], DDX proteins were eluted using 0–0.25 M imidazole gradients, and protein presence in each fraction was assayed *via* SDS-PAGE followed by Coomassie staining. Pooled fractions of proteins were dialyzed against Heparin Column buffer A [20 mM Tris (pH 7.8), 75 mM NaCl, 1 mM EDTA, 1 mM TCEP, and 2% glycerol] and further purified on a 5 ml HiTrap Heparin Column (GE Healthcare) and eluted using a 75 mM to 2 M NaCL gradient. Purified DDX proteins were dialyzed against Heparin Buffer A and cleaved by Tev protease (1:20 mass ratio) overnight. The resultant DDX proteins were further purified from the HisMBP tag and Tev protease *via* Heparin column as described above.

RNA production

Stem IIB, poly(U)21, FAM-labeled 10mer, Dab-labeled 26mer, and 14mer RNA oligomers were purchased from Thermo Fisher. Full-length RRE RNAs used for EMSA or TIRF experiments were produced as previously described [24,53,54].

ATPase activity assay

DDX21 ATPase activity was measured using an NADH-coupled ATPase assay as previously described [36]. Reaction mixtures were monitored for the depletion of NADH by measuring $Abs_{(340)}$ with an Envision 2104 MultiPlate Reader (PerkinElmer). Fifty microliter reactions contained 10 µM DDX21, 20 mM Tris (pH 7.5), 60 mM NaCl, 55 mM KCl, 2 mM $MgCl_2$, 5% glycerol, and 0.1 mg/ml bovine serum albumin. The reactions with either increasing amounts of ATP or RNA were carried out at room temperature in UV-transparent 96-well plates (Grenier Bio-one), and the hydrolysis rates were analyzed using Michaelis–Menten equations. Because it is difficult to accurately measure the path length of a 50 µl reaction volume, a concentration-dependent standard curve of NADH was generated in the same 50 µl buffer to convert OD_{340} to an NADH molar value, resulting in a value of 1abs unit equaling 0.98 ± 0.006 mM NADH. Pyruvate kinase, lactate dehydrogenase, and ATP were purchased from Sigma. Phosphoenolpyruvate was purchased from Santa Cruz Biotechnology.

Fluorescence-based helicase assay

DDX21 RNA unwinding activity assay was adapted from previous work and was measured in real time using an Envision 2104 MultiPlate Reader (PerkinElmer) [39] Fifty microliter reaction mixtures consisted of a 20 nM pre-formed RNA duplex (FAM--labeled 10mer and DAB-labeled 26mer), 100 nM 14mer RNA competitor, 2 µM DDX21 or DDX21(183–620), 1× helicase buffer [20 mM Tris (pH 7.5), 60 mM NaCl, 55 mM KCl, 2 mM $MgCl_2$, and 0.67 U/µl RNaseOUT), and 0 or 1 mM ATP. The resulting fluorescence data were fitted as previously

described using Igor (Wavemetrics) to the following equation

$$F(t) = F_0 + (F_\infty - F_0)(1 - \exp(-k_{unw}t))$$

where $F(t)$ is fluorescent signal at any given time (t), F_0 is initial fluorescent signal, F_∞ is maximal fluorescent signal, and k_{unw} is the unwinding rate constant [39].

Fluorescence polarization assay

Fluorescence polarization binding assays were conducted as previously described [13,24]. All Rev constructs were fluorescently labeled as previously described using maleimide-alexa555 (Invitrogen) [24]. Reaction conditions contained 15 nM Rev-alexa555 (or mutants). Samples were prepared in 96-well black plate (Grenier), and polarization was measured using Envision 2104 MultiPlate Reader (PerkinElmer). The average polarization values were calculated from seven consecutive readings of each plate. Equilibrium K_d values were determined by fitting to quadratic equations using Igor (Wavemetrics) as described previously [13].

Co-IP assay and Western blotting

For production of DEAD-box and Rev-producing cells, Flp-In T-Rex-GagRRE-HeLa cells (~ 1.5×10^6) were seeded and transduced with various lentiviruses as indicated in the text and Fig. 6. After 24 h, doxycycline was added to 1 μg/ml. Cells were grown for an additional 24 h at 37 °C to induce the expression of GagRRE mRNA and were then harvested using trypsin digestion. For IP, cell pellets were resuspended with IP buffer [50 mM Tris (pH 7.4), 75 mM NaCl, 1 mM $MgCl_2$, 1% Nonidet P-40, 1 mM DTT, 1 mM phenylmethylsulfonyl fluoride, and complete protease inhibitor cocktail (EDTA-free, Roche Diagnostics)] [2]. Where indicated, cell lysates were treated with 50 μg/ml RNase A (Amresco) at 37 °C for 30 min. Lysates were cleared by centrifugation at 10,000*g* for 10 min at 4 °C. An aliquot of the supernatant was saved for Western blotting ("input"), while the remainder was used for a 30 min IP incubation with the following antibodies: rabbit IgG (Cell Signaling Technology), rabbit α-DDX21 IgG (10528-1-AP; Proteintech, Rosemond, IL), mouse α-DDX3 IgG (ab50703; Abcam), and rabbit α-DDX1 IgG (11357-1-AP; Proteintech). The lysate–antibody mixtures were then incubated with protein-G Dynabeads (Life Technologies) for 30 min. Beads were washed three times with wash buffer [50 mM Tris (pH 7.4), 75 mM NaCl, 1 mM $MgCl_2$, 0.05% Triton X-100], and bound proteins were eluted with SDS sample buffer. Protein samples were resolved by SDS-PAGE and transferred to nitrocellulose membranes (Amersham Biosciences). Mouse α-V5 antibody (R960-25; Life Technologies) was used to detect Rev-GFP-V5 (WT or V16D), DDX21, and DDX1, while DDX3 was detected using the α-DDX3 antibody noted above.

Electromobility shift assay (EMSA)

Radioactive EMSA assays (including radiolabeling of RRE and buffer preparation) were performed as previously described [24]. UV-visualized EMSA assays were adapted from previous protocols as follows [43]: 20 μl reaction mixtures containing varying DDX21 or Rev concentrations, 12.5 nM RRE RNA, 1× reaction buffer [50 mM Tris (pH 7.5), 150 mM KCl, 10% glycerol, 1% Triton X-100, 0.1 mg/ml bovine serum albumin, and 0.67 U/μl RNaseOUT], and DEPC-treated H_2O were incubated at room temperature for 30 min to come to binding equilibrium. Reactions were then loaded onto a 10% TBE polyacrylamide gel (Invitrogen) and run for 2 h at 200 V. Gels were soaked in SYBRGold Stain (Invitrogen) for 30 min, and RNA was visualized using a BioRad Gel Doc EZ Imager™. Image contrast was adjusted slightly using photoshop (Adobe®).

TIRF microscopy of Rev oligomerization

The full-length RRE (351 nt) containing extensions at both the 3′ and 5′ ends was transcribed *in vitro* from an appropriate DNA template using T7 RNA polymerase as previously described [23]. A biotinylated DNA oligonucleotide (28 nt) was hybridized at the 3′ end of the RRE transcript for surface immobilization. RRE–DNA hybrid (500 pM) was immobilized on a streptavidin-coated quartz surface, as described elsewhere [14,23,46]. The quartz surface was passivated with polyethylene glycol to inhibit nonspecific adsorption of Rev or DDX proteins, as described [55]. Rev was labeled with A555 at a single N-terminal cysteine, as described [14]. A555-Rev (1 nm) with or without 150 nM DDX protein, in 50 mM Hepes buffer (pH 7.5) containing 2 mM Trolox, 150 mm KCl, 10 mM K_2SO_4, 2 mM $MgCl_2$, 2 mM DTT, and oxygen scavenging system (50 μg/ml glucose oxidase, 10 μg/ml catalase, and 2–5% wt/vol glucose) [55], was introduced into the surrounding solution. The A555 fluorophore was excited using a 532-nm laser in a custom-built prism-based TIRF microscope. Emission from A555 was collected through a water immersion objective and recorded on an intensified CCD camera with 100-ms time resolution [56,57]. A single-molecule data acquisition package (downloaded from https://physics.illinois.edu/cplc/software/) was used to record data. Fluorescence intensity traces from individual Rev–RRE complexes were extracted from the CCD camera movie files and processed using a custom program written in Matlab. All intensity time traces were corrected for background and smoothed using 3-point linear averaging. Multiple time traces (> 100) were used to generate fluorescence intensity histograms using

Matlab and Igor Pro software (WaveMetrics). Individual time traces were fitted using Hidden Markov modeling [58] to determine the dwell times spent in one state prior to transition to another state. The information from multiple times traces was compiled in the form of dwell time histograms, which were fitted with exponential functions to determine the rate constants for transitions from one state to another, using Igor Pro software (WaveMetrics).

Acknowledgments

Funding for this work was provided by the National Institute of General Medical Sciences (Grant P50 GM082545; W. Sundquist PI, to J.R.W, D.P.M., and L.G.), the American Cancer Society (fellowship award 121633-PF-11-222-01-RMC to J.A.H.), and California HIV/AIDS Research Program (fellowship award F12-SRI-210 to R.L.; fellowship award F12-SRI-203 to L.Z.). Thank you to Katrina Schreiber for editing this manuscript.

Received 18 May 2017;
Received in revised form 26 June 2017;
Accepted 27 June 2017
Available online 10 July 2017

Keywords:
RNA structure;
HIV-1;
RRE;
Rev;
DEAD-box protein

These authors contributed equally to this work.

Abbreviations used:
Rev, regulator of expression of virion proteins; RRE, Rev-responsive element; RCCs, Rev-containing complexes; NIS, nuclear diffusion inhibitory signal; TIRF, total internal reflection fluorescence; IP, immunoprecipitation; NLS, nuclear localization signal; NES, nuclear export signal.

References

[1] M. Fornerod, M. Ohno, M. Yoshida, I.W. Mattaj, CRM1 is an export receptor for leucine-rich nuclear export signals, Cell 90 (1997) 1051–1060.
[2] C. Jain, J.G. Belasco, Structural model for the cooperative assembly of HIV-1 Rev multimers on the RRE as deduced from analysis of assembly-defective mutants, Mol. Cell 7 (2001) 603–614.
[3] M.D. Daugherty, I. D'Orso, A.D. Frankel, A solution to limited genomic capacity: using adaptable binding surfaces to assemble the functional HIV Rev oligomer on RNA, Mol. Cell 31 (2008) 824–834.
[4] B. Jayaraman, D.C. Crosby, C. Homer, I. Ribeiro, D. Mavor, A.D. Frankel, RNA-directed remodeling of the HIV-1 protein Rev orchestrates assembly of the Rev–Rev response element complex, Elife 3 (2014), e04120.
[5] M.A. DiMattia, N.R. Watts, S.J. Stahl, C. Rader, P.T. Wingfield, D.I. Stuart, et al., Implications of the HIV-1 Rev dimer structure at 3.2 A resolution for multimeric binding to the Rev response element, Proc. Natl. Acad. Sci. U. S. A. 107 (2010) 5810–5814.
[6] M.H. Malim, J. Hauber, S.Y. Le, J.V. Maizel, B.R. Cullen, The HIV-1 Rev trans-activator acts through a structured target sequence to activate nuclear export of unspliced viral mRNA, Nature 338 (1989) 254–257.
[7] M.H. Malim, B.R. Cullen, HIV-1 structural gene expression requires the binding of multiple Rev monomers to the viral RRE: implications for HIV-1 latency, Cell 65 (1991) 241–248.
[8] L.S. Tiley, M.H. Malim, H.K. Tewary, P.G. Stockley, B.R. Cullen, Identification of a high-affinity RNA-binding site for the human immunodeficiency virus type 1 Rev protein, Proc. Natl. Acad. Sci. U. S. A. 89 (1992) 758–762.
[9] C. Jain, J.G. Belasco, A structural model for the HIV-1 Rev–RRE complex deduced from altered-specificity Rev variants isolated by a rapid genetic strategy, Cell 87 (1996) 115–125.
[10] S. Naji, G. Ambrus, P. Cimermancic, J.R. Reyes, J.R. Johnson, R. Filbrandt, et al., Host cell interactome of HIV-1 Rev includes RNA helicases involved in multiple facets of virus production, Mol. Cell. Proteomics 11 (2012) (M111 015313).
[11] J. Popow, J. Jurkin, A. Schleiffer, J. Martinez, Analysis of orthologous groups reveals archease and DDX1 as tRNA splicing factors, Nature 511 (2014) 104–107.
[12] M.H. Lin, H. Sivakumaran, A. Jones, D. Li, C. Harper, T. Wei, et al., A HIV-1 Tat mutant protein disrupts HIV-1 Rev function by targeting the DEAD-box RNA helicase DDX1, Retrovirology 11 (2014) 121.
[13] S.P. Edgcomb, A.B. Carmel, S. Naji, G. Ambrus-Aikelin, J.R. Reyes, A.C. Saphire, et al., DDX1 is an RNA-dependent ATPase involved in HIV-1 Rev function and virus replication, J. Mol. Biol. 415 (2012) 61–74.
[14] R.M. Robertson-Anderson, J. Wang, S.P. Edgcomb, A.B. Carmel, J.R. Williamson, D.P. Millar, Single-molecule studies reveal that DEAD box protein DDX1 promotes oligomerization of HIV-1 Rev on the Rev response element, J. Mol. Biol. 410 (2011) 959–971.
[15] J. Fang, E. Acheampong, R. Dave, F. Wang, M. Mukhtar, R.J. Pomerantz, The RNA helicase DDX1 is involved in restricted HIV-1 Rev function in human astrocytes, Virology 336 (2005) 299–307.
[16] A. Brai, R. Fazi, C. Tintori, C. Zamperini, F. Bugli, M. Sanguinetti, et al., Human DDX3 protein is a valuable target to develop broad spectrum antiviral agents, Proc. Natl. Acad. Sci. U. S. A. 113 (2016) 5388–5393.
[17] A. Frohlich, B. Rojas-Araya, C. Pereira-Montecinos, A. Dellarossa, D. Toro-Ascuy, Y. Prades-Perez, et al., DEAD-box RNA helicase DDX3 connects CRM1-dependent nuclear export and translation of the HIV-1 unspliced mRNA through its N-terminal domain, Biochim. Biophys. Acta 1859 (2016) 719–730.
[18] R. Soto-Rifo, P.S. Rubilar, T. Ohlmann, The DEAD-box helicase DDX3 substitutes for the cap-binding protein eIF4E to promote compartmentalized translation initiation of the HIV-1 genomic RNA, Nucleic Acids Res. 41 (2013) 6286–6299.

[19] M. Yasuda-Inoue, M. Kuroki, Y. Ariumi, DDX3 RNA helicase is required for HIV-1 Tat function, Biochem. Biophys. Res. Commun. 441 (2013) 607–611.
[20] M. Yasuda-Inoue, M. Kuroki, Y. Ariumi, Distinct DDX DEAD-box RNA helicases cooperate to modulate the HIV-1 Rev function, Biochem. Biophys. Res. Commun. 434 (2013) 803–808.
[21] M.C. Lai, S.W. Wang, L. Cheng, W.Y. Tarn, S.J. Tsai, H.S. Sun, Human DDX3 interacts with the HIV-1 Tat protein to facilitate viral mRNA translation, PLoS One 8 (2013), e68665.
[22] M. Ishaq, J. Hu, X. Wu, Q. Fu, Y. Yang, Q. Liu, et al., Knockdown of cellular RNA helicase DDX3 by short hairpin RNAs suppresses HIV-1 viral replication without inducing apoptosis, Mol. Biotechnol. 39 (2008) 231–238.
[23] R. Lamichhane, J.A. Hammond, R.F. Pauszek III, R.M. Anderson, I. Pedron, E. van der Schans, et al., A DEAD-box protein acts through RNA to promote HIV-1 Rev–RRE assembly, Nucleic Acids Res 45 (2017) 4632–4641.
[24] J.A. Hammond, R. Lamichhane, D.P. Millar, J.R. Williamson, A DEAD-box helicase mediates an RNA structural transition in the HIV-1 Rev response element, J. Mol. Biol. 429 (2017) 697–714.
[25] Y. Zhang, K.C. Baysac, L.F. Yee, A.J. Saporita, J.D. Weber, Elevated DDX21 regulates c-Jun activity and rRNA processing in human breast cancers, Breast Cancer Res. 16 (2014) 449.
[26] Y. Jung, S. Lee, H.S. Choi, S.N. Kim, E. Lee, Y. Shin, et al., Clinical validation of colorectal cancer biomarkers identified from bioinformatics analysis of public expression data, Clin. Cancer Res. 17 (2011) 700–709.
[27] D. Henning, R.B. So, R. Jin, L.F. Lau, B.C. Valdez, Silencing of RNA helicase II/Gualpha inhibits mammalian ribosomal RNA production, J. Biol. Chem. 278 (2003) 52307–52314.
[28] E. Calo, R.A. Flynn, L. Martin, R.C. Spitale, H.Y. Chang, J. Wysocka, RNA helicase DDX21 coordinates transcription and ribosomal RNA processing, Nature 518 (2015) 249–253.
[29] K.E. Sloan, M.S. Leisegang, C. Doebele, A.S. Ramirez, S. Simm, C. Safferthal, et al., The association of late-acting snoRNPs with human pre-ribosomal complexes requires the RNA helicase DDX21, Nucleic Acids Res. 43 (2015) 553–564.
[30] G. Chen, C.H. Liu, L. Zhou, R.M. Krug, Cellular DDX21 RNA helicase inhibits influenza A virus replication but is counteracted by the viral NS1 protein, Cell Host Microbe 15 (2014) 484–493.
[31] Z. Zhang, T. Kim, M. Bao, V. Facchinetti, S.Y. Jung, A.A. Ghaffari, et al., DDX1, DDX21, and DHX36 helicases form a complex with the adaptor molecule TRIF to sense dsRNA in dendritic cells, Immunity 34 (2011) 866–878.
[32] P. Linder, E. Jankowsky, From unwinding to clamping—the DEAD box RNA helicase family, Nat. Rev. Mol. Cell Biol. 12 (2011) 505–516.
[33] B.C. Valdez, D. Henning, K. Perumal, H. Busch, RNA-unwinding and RNA-folding activities of RNA helicase II/Gu—two activities in separate domains of the same protein, Eur. J. Biochem./FEBS 250 (1997) 800–807.
[34] B.C. Valdez, Structural domains involved in the RNA folding activity of RNA helicase II/Gu protein, Eur. J. Biochem./FEBS 267 (2000) 6395–6402.
[35] A. Garbelli, S. Beermann, G. Di Cicco, U. Dietrich, G. Maga, A motif unique to the human DEAD-box protein DDX3 is important for nucleic acid binding, ATP hydrolysis, RNA/DNA unwinding and HIV-1 replication, PLoS One 6 (2011), e19810.
[36] J.G. Norby, Coupled assay of Na+,K+-ATPase activity, Methods Enzymol. 156 (1988) 116–119.
[37] C.G. Lee, J. Hurwitz, A new RNA helicase isolated from HeLa cells that catalytically translocates in the 3′ to 5′ direction, J. Biol. Chem. 267 (1992) 4398–4407.
[38] C.G. Noble, H. Song, MLN51 stimulates the RNA-helicase activity of eIF4AIII, PLoS One 2 (2007), e303.
[39] T. Bizebard, M. Dreyfus, A FRET-based, continuous assay for the helicase activity of DEAD-box proteins, Methods Mol. Biol. 1259 (2015) 199–209.
[40] J. Fang, S. Kubota, B. Yang, N. Zhou, H. Zhang, R. Godbout, et al., A DEAD box protein facilitates HIV-1 replication as a cellular co-factor of Rev, Virology 330 (2004) 471–480.
[41] S.P. Edgcomb, A. Aschrafi, E. Kompfner, J.R. Williamson, L. Gerace, M. Hennig, Protein structure and oligomerization are important for the formation of export-competent HIV-1 Rev–RRE complexes, Protein Sci. 17 (2008) 420–430.
[42] S.L. Thomas, M. Oft, H. Jaksche, G. Casari, P. Heger, M. Dobrovnik, et al., Functional analysis of the human immunodeficiency virus type 1 Rev protein oligomerization interface, J. Virol. 72 (1998) 2935–2944.
[43] X. Fang, J. Wang, I.P. O'Carroll, M. Mitchell, X. Zuo, Y. Wang, et al., An unusual topological structure of the HIV-1 Rev response element, Cell 155 (2013) 594–605.
[44] M.D. Daugherty, D.S. Booth, B. Jayaraman, Y. Cheng, A.D. Frankel, HIV Rev response element (RRE) directs assembly of the Rev homooligomer into discrete asymmetric complexes, Proc. Natl. Acad. Sci. U. S. A. 107 (2010) 12481–12486.
[45] M.D. Daugherty, B. Liu, A.D. Frankel, Structural basis for cooperative RNA binding and export complex assembly by HIV Rev, Nat. Struct. Mol. Biol. 17 (2010) 1337–1342.
[46] S.J. Pond, W.K. Ridgeway, R. Robertson, J. Wang, D.P. Millar, HIV-1 Rev protein assembles on viral RNA one molecule at a time, Proc. Natl. Acad. Sci. U. S. A. 106 (2009) 1404–1408.
[47] A.A. Putnam, E. Jankowsky, DEAD-box helicases as integrators of RNA, nucleotide and protein binding, Biochim. Biophys. Acta 2013 (1829) 884–893.
[48] H. Flores-Rozas, J. Hurwitz, Characterization of a new RNA helicase from nuclear extracts of HeLa cells which translocates in the 5′ to 3′ direction, J. Biol. Chem. 268 (1993) 21372–21383.
[49] K.H. Nielsen, H. Chamieh, C.B. Andersen, F. Fredslund, K. Hamborg, H. Le Hir, et al., Mechanism of ATP turnover inhibition in the EJC, RNA 15 (2009) 67–75.
[50] R.J. Pomerantz, T. Seshamma, D. Trono, Efficient replication of human immunodeficiency virus type 1 requires a threshold level of Rev: potential implications for latency, J. Virol. 66 (1992) 1809–1813.
[51] M. Beck, A. Schmidt, J. Malmstroem, M. Claassen, A. Ori, A. Szymborska, et al., The quantitative proteome of a human cell line, Mol. Syst. Biol. 7 (2011) 549.
[52] H. Wodrich, J. Bohne, E. Gumz, R. Welker, H.G. Krausslich, A new RNA element located in the coding region of a murine endogenous retrovirus can functionally replace the Rev/Rev-responsive element system in human immunodeficiency virus type 1 Gag expression, J. Virol. 75 (2001) 10670–10682.
[53] J.A. Hammond, R.P. Rambo, J.S. Kieft, Multi-domain packing in the aminoacylatable 3′ end of a plant viral RNA, J. Mol. Biol. 399 (2010) 450–463.

[54] J.A. Hammond, R.P. Rambo, M.E. Filbin, J.S. Kieft, Comparison and functional implications of the 3D architectures of viral tRNA-like structures, RNA 15 (2009) 294–307.
[55] R. Lamichhane, G.M. Daubner, J. Thomas-Crusells, S.D. Auweter, C. Manatschal, K.S. Austin, et al., RNA looping by PTB: evidence using FRET and NMR spectroscopy for a role in splicing repression, Proc. Natl. Acad. Sci. U. S. A. 107 (2010) 4105–4110.
[56] R. Lamichhane, S.Y. Berezhna, J.P. Gill, E. Van der Schans, D.P. Millar, Dynamics of site switching in DNA polymerase, J. Am. Chem. Soc. 135 (2013) 4735–4742.
[57] S.Y. Berezhna, J.P. Gill, R. Lamichhane, D.P. Millar, Single-molecule Forster resonance energy transfer reveals an innate fidelity checkpoint in DNA polymerase I, J. Am. Chem. Soc. 134 (2012) 11261–11268.
[58] S.A. McKinney, C. Joo, T.J. Ha, Analysis of single-molecule FRET trajectories using hidden markov modeling, J. Biophys. 91 (2006) 1941–1951.